TITLE:

Multiradar Data Fusion for Respiratory Measurement of Multiple People

AUTHOR(S):

Iwata, Shunsuke; Koda, Takato; Sakamoto, Takuya

CITATION:

Iwata, Shunsuke ...[et al]. Multiradar Data Fusion for Respiratory Measurement of Multiple People. IEEE Sensors Journal 2021, 21(22): 25870-25879

ISSUE DATE:

2021-11-15

URL:

http://hdl.handle.net/2433/277782

RIGHT:

This work is licensed under a Creative Commons Attribution 4.0 License

京都大学学術情報リポジトリ
KURENAI
Kyoto University Research Information Repository

京都大学 KYOTO UNIVERSITY
A Self-archived copy in
Kyoto University Research Information Repository
https://repository.kulib.kyoto-u.ac.jp
京都大学学術情報リポジトリ KURENAI 紅 Kyoto University Research Information Repository

IEEE Sensors Council

Multiradar Data Fusion for Respiratory Measurement of Multiple People

Shunsuke Iwata, *Member, IEEE*, Takato Koda, and Takuya Sakamoto, *Senior Member, IEEE*

***Abstract*—This study proposes a data fusion method for multiradar systems to enable measurement of the respiration of multiple people located at arbitrary positions. Using the proposed method, the individual respiration rates of multiple people can be measured, even when echoes from some of these people cannot be received by one of the radar systems because of shadowing. In addition, the proposed method does not require information about the positions and orientations of the radar systems used because the method can estimate the layout of these radar systems by identifying multiple human targets that can be measured from different angles using multiple radar systems. When a single target person can be measured using multiple radar systems simultaneously, the proposed method selects an accurate signal from among the multiple signals based on the spectral characteristics. To verify the effectiveness of the proposed method, we performed experiments based on two scenarios with different layouts that involved seven participants and two radar systems. Through these experiments, the proposed method was demonstrated to be capable of measuring the respiration of all seven people by overcoming the shadowing issue. In the two scenarios, the average errors of the proposed method in estimating the respiration rates were 0.33 and 1.24 respirations per minute (rpm), respectively, thus demonstrating accurate and simultaneous respiratory measurements of multiple people using the multiradar system.**

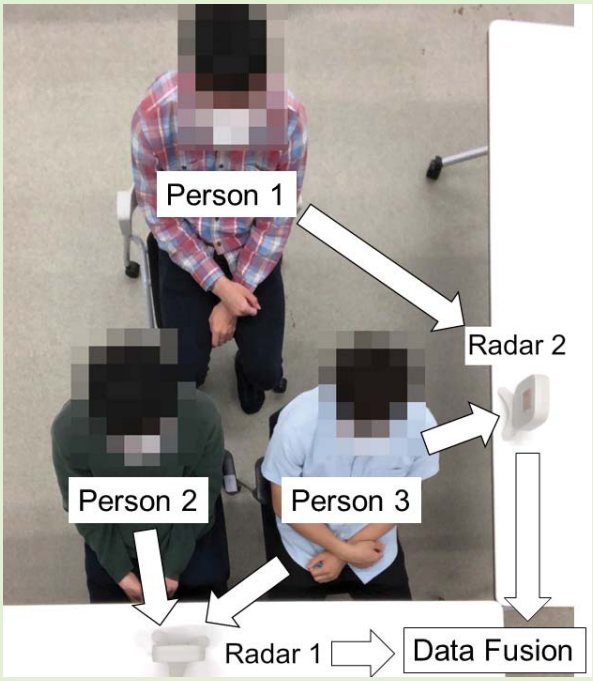

***Index Terms*—Biomedical engineering, data fusion, radar measurement, radar imaging, radar signal processing.**

I. Introduction

RESPIRATORY measurements have become increasingly important in a variety of applications, including healthcare, home medication, medical alert systems for babies, and monitoring systems for infants and senior citizens. To monitor patient respiration in such applications, many sensors and systems have been developed [1]–[3]. Systems that use radar are particularly promising because there is no need for the patient to wear a device. As a result, respiration can be measured over the long term without causing patient discomfort. A number of existing studies have been reported on the measurement of people using radar techniques, including systems for the estimation of the locations of people [4]–[9], tracking of people in motion [10]–[17], posture recognition [18]–[20], and detection of patient vital signs, including heartbeat and respiration [21]–[41].

Another advantage of radar-based respiratory measurement is the possibility of performing simultaneous measurements of the respiration of multiple people using only a single device. There have been numerous studies in which a single-radar system has been used to measure the respiration of multiple people [21]–[39]. For example, Nosrati *et al.* [36], Islam *et al.* [37], Su *et al.* [38], and Koda *et al.* [39] used single-radar systems to demonstrate simultaneous measurement of the respiration of two, three, three, and seven people, respectively. These studies, however, did not consider the

Manuscript received August 1, 2021; revised September 30, 2021; accepted October 1, 2021. Date of publication October 4, 2021; date of current version November 12, 2021. This work was supported in part by the Japan Society for the Promotion of Science (JSPS) KAKENHI under Grant 19H02155 and Grant 21H03427, in part by the Japan Science and Technology Agency (JST) Promoting Individual Research to Nurture the Seeds of Future Innovation and Organizing Unique, Innovative Network (PRESTO) under Grant JPMJPR1873, and in part by JST Center of Innovation (COI) under Grant JPMJCE1307. The associate editor coordinating the review of this article and approving it for publication was Dr. Michail Antoniou. *(Corresponding author: Takuya Sakamoto.)*

This work involved human subjects or animals in its research. Approval of all ethical and experimental procedures and protocols was granted by the Ethics Committee of the Graduate School of Engineering, Kyoto University under Application No. 201916.

The authors are with the Department of Electrical Engineering, Graduate School of Engineering, Kyoto University, Kyoto 615-8510, Japan (e-mail: sakamoto.takuya.8n@kyoto-u.ac.jp).

Digital Object Identifier 10.1109/JSEN.2021.3117707

This work is licensed under a Creative Commons Attribution 4.0 License. For more information, see https://creativecommons.org/licenses/by/4.0/

京都大学 KYOTO UNIVERSITY
A Self-archived copy in
Kyoto University Research Information Repository
https://repository.kulib.kyoto-u.ac.jp
京都大学学術情報リポジトリ KURENAI 紅 Kyoto University Research Information Repository

effect of the shadowing problem, in which an echo from one target person is blocked by another person located between the first person and the radar system; this results in the radar system being unable to detect a person (or some people) when multiple people are present in the scene.

To overcome the shadowing problem, this study introduces simultaneous use of multiple radar systems to perform respiratory measurements of multiple people. There have been previous studies that used multiradar systems to measure the respiration of multiple people: Shang *et al.* [40] used two radar systems to measure two people in the presence of body motion, and Yang *et al.* [41] used two radar systems to measure five people. In these studies, it was assumed that the relative positions and orientations of the radar systems were known in advance, and that the echoes from all target people could be measured directly by each of the radar systems without the shadowing problem. These assumptions, however, cannot always be satisfied in practice, which hinders the use of the radar-based respiratory measurement approach in actual daily environments.

As discussed above, none of the existing studies have accounted for the effect of the shadowing problem, which prevents the echo from one person from being detected by one of the radar systems. In this study, we propose a novel multiradar data fusion method to perform respiratory measurements that can measure multiple people simultaneously. The proposed method can mitigate the effect of the shadowing problem using multiple radar systems without knowing the relative locations and orientations of these radar systems. The proposed method generates multiple radar images using the multiradar data, and these radar images are then converted into multiple sets of two-dimensional point clouds. To align these point clouds, the proposed method then estimates the relative positions and orientations of the radar systems, which allows for data fusion in the multiradar system and thus overcomes the shadowing problem. The proposed method even works when the positional relationships among the radar systems are unknown, which means that there is no requirement for calibration to be performed beforehand and no restriction on the physical installation of the radar systems. The performance of the proposed method is evaluated quantitatively by performing radar measurements involving seven participants and a pair of radar systems.

The main contributions of this study are as follows:

- This study proposes a method that enables the respiratory measurement of multiple people, even when some of them cannot be directly measured because of shadowing.
- Using the method proposed in this study, the relative positions and orientations of several radar systems are automatically estimated through the measurement of multiple people.
- The proposed method improves the estimation accuracy of respiration by integrating data from multiple radar systems.

These issues have not yet been addressed by existing studies, including ours [39], which demonstrates the novelty and innovation of this work. Table I compares this study and other existing studies. A preprint of this manuscript has been posted [42].

TABLE I
COMPARISON OF THIS STUDY WITH EXISTING STUDIES

Ref. no.	Center freq. (GHz)	No. of radar systems	No. of target people	Shadowing issues resolved	Layout of radar systems
[36]	2.4	1	2	No	–
[37]	24.0	1	3	No	–
[38]	9.0	1	3	No	–
[39]	79.0	1	7	No	–
[40]	3.2	2	2	No	Known
[41]	8.1	2	2-5	No	Known
This work	79.0	2	7	Yes	Unknown

II. IMAGING AND CLUSTERING OF HUMAN TARGETS USING MULTIPLE RADAR SYSTEMS

We assume use of a multiradar system comprising M radar systems with positions and angles that are unknown. Each radar system contains a K-element array (or virtual array). Let $s_k(t, r)$ denote the signal received by the k-th element ($k = 0, 1, \ldots, K-1$) of the array, where t is the slow time and the range r is expressed as $r = ct'/2$ using the fast time t' and speed of light c. A signal vector $\boldsymbol{s}(t, r)$ is defined as $\boldsymbol{s}(t, r) = [s_0(t, r), s_1(t, r), \ldots, s_{K-1}(t, r)]^{\mathrm{T}}$, where the superscript T represents a transpose operator. We assume here that all elements of the array antennas are calibrated and that static clutter is suppressed by subtracting the time-averaged signal.

Using the m-th radar system ($m = 1, \ldots, M$), a radar image is generated and is expressed in the two-dimensional Cartesian coordinate system (x_m, y_m), where the x_m axis is aligned with the array baseline of the m-th radar system. A complex radar image $I_m(t, \boldsymbol{r}_m)$ is generated from the m-th radar system's data as $I_m(t, \boldsymbol{r}_m) = \boldsymbol{w}(\phi_m)^{\mathrm{H}} \boldsymbol{s}(t, \rho_m)$, where the superscript H represents a conjugate transpose operator and $\boldsymbol{r}_m$ is the position vector that can be expressed as (x_m, y_m) in Cartesian coordinates and as (ρ_m, ϕ_m) in polar coordinates. The weight vector is $\boldsymbol{w}(\theta) = [w_0, w_1, \ldots, w_{K-1}]^{\mathrm{T}}$, where the choice of w_k depends on the imaging algorithm being used. In this study, we use a straightforward beamformer (BF) method for simplicity, in which the weights are set as $w_k(\theta) = \alpha_k \mathrm{e}^{\mathrm{j}(2\pi d_k/\lambda)\cos\theta}$ ($k = 0, 1, \ldots, K-1$), where d_k is the x_m coordinate of the k-th element of the array. Here, we use the Taylor window coefficient α_k. Fig. 1 shows a system model containing multiple radar systems for measurement of multiple human targets, in which we see that each radar system has its own coordinate system.

Next, using each radar image $|I_m(t, \boldsymbol{r}_m)|^2$, a point cloud is generated according to [39]. The X-means clustering technique [39], [43] is then applied to the point cloud and the clusters $c_1, c_2, \ldots, c_{N_m}$ are generated; these clusters correspond to the N_m targets. Note that N_m is the number of targets detected using the m-th radar system. For presentation purposes, we generated a radar cluster image $C_m(t, \boldsymbol{r}_m)$ that takes the values $\{0, 1, 2, \ldots, N_m\}$, which correspond to the indices of the clusters $c_1, c_2, \ldots, c_{N_m}$ except for 0; $C_m(t, \boldsymbol{r}_m) = 0$ indicates that no cluster is associated with $\boldsymbol{r}_m$. Finally, the representative position $\boldsymbol{r}_m^{(n)}$ of cluster c_n in the m-th radar image is calculated [39]; the clusters' representative positions are

京都大学 KYOTO UNIVERSITY
A Self-archived copy in
Kyoto University Research Information Repository
https://repository.kulib.kyoto-u.ac.jp
京都大学学術情報リポジトリ KURENAI Kyoto University Research Information Repository

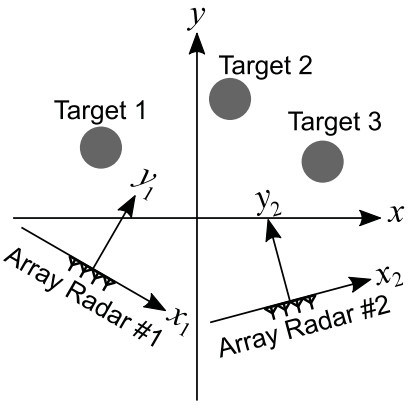

Fig. 1. System model for measuring multiple target people using multiple radar systems.

then processed in the proposed data fusion algorithm, which combines multiple radar images.

III. Multiradar Data Fusion for Respiratory Measurement of Multiple People

The main issue when performing radar measurements of multiple human targets is that not all of these human targets can be measured directly using only a single radar system because of shadowing, i.e., where one human echo is blocked by another human target or by obstacles; this occurs frequently when multiple people are located together and are densely spaced. To mitigate this issue, we use a multiradar system to increase the probability that at least one of these radar systems can detect each of the human targets in the scene. Given the radar images $I_m(t, \boldsymbol{r}_m)$ and the cluster positions $\boldsymbol{r}_m^{(n)}$ for $m = 1, \ldots, M$, we propose a data fusion method here that combines the multiple radar images. Here, we assume a special case with $M = 2$ for simplicity. The first step in the method is to find a rigid transformation that can align the coordinates from the x_2–y_2 coordinate system to those of the x_1–y_1 coordinate system.

A. Procrustes Analysis for Alignment of the Associated Target Clusters

We propose a data fusion method that uses Procrustes analysis [44] to find the rigid transformation parameters required to describe the relationship between two sets of points in a plane. In this study, Procrustes analysis is chosen because it is known as one of the standard algorithms for estimating the relative position and orientation of a pair of images when the corresponding points are given. In addition, because the model of Procrustes analysis is linear, the solution can be obtained without initial approximation of the unknown parameters unlike iterative closest point (ICP) algorithm [45]. Let us assume here that N' pairs of two-dimensional vectors $(\boldsymbol{r}_1^{(1)}, \boldsymbol{r}_2^{(1)}), (\boldsymbol{r}_1^{(2)}, \boldsymbol{r}_2^{(2)}), \ldots, (\boldsymbol{r}_1^{(N')}, \boldsymbol{r}_2^{(N')})$ correspond to N' pairs of points, and that $N' \leq \min(N_1, N_2)$ is satisfied. The purpose of this section is to find a rigid transformation that adjusts the points $\boldsymbol{r}_2^{(n)}$ with respect to $\boldsymbol{r}_1^{(n)}$ $(n = 1, \ldots, N')$. If appropriate transformation parameters are selected, the points are then transformed to satisfy $\boldsymbol{r}_1^{(n)} \simeq R\boldsymbol{r}_2^{(n)} + \boldsymbol{t}$ using the translation vector $\boldsymbol{t}$ and the rotation matrix R. If we subtract the average coordinates $\bar{\boldsymbol{r}}_m = (1/N') \sum_{n=1}^{N'} \boldsymbol{r}_m^{(n)}$ $(m = 1, 2)$ from the position vectors using $\tilde{\boldsymbol{r}}_m^{(n)} = \boldsymbol{r}_m^{(n)} - \bar{\boldsymbol{r}}_m$, we can then simplify the problem for large N'; we need only estimate the R that satisfies $\tilde{\boldsymbol{r}}_1^{(n)} = R\tilde{\boldsymbol{r}}_2^{(n)}$. Here, we define $2 \times N'$ matrices S_1 and S_2 as:

$$S_1 = [\tilde{\boldsymbol{r}}_1^{(1)}, \tilde{\boldsymbol{r}}_1^{(2)}, \ldots, \tilde{\boldsymbol{r}}_1^{(N')}], \tag{1}$$

$$S_2 = [\tilde{\boldsymbol{r}}_2^{(1)}, \tilde{\boldsymbol{r}}_2^{(2)}, \ldots, \tilde{\boldsymbol{r}}_2^{(N')}], \tag{2}$$

and we estimate a rotation matrix R^* as:

$$R^* = \arg\min_R \|S_1 - RS_2\|_{\mathrm{F}}^2, \quad \text{subject to } R^{\mathrm{T}}R = I, \det R = 1, \tag{3}$$

where the subscripted F denotes the Frobenius norm and represents the square root of the sum of squares of all components.

In Procrustes analysis, rather than solving for the optimization problem in Eq. (3) directly, singular value decomposition is used to estimate R^*; $S_1 S_2^{\mathrm{T}}$ is decomposed using the form $S_1 S_2^{\mathrm{T}} = U \Sigma V^{\mathrm{T}}$, where U and V are 2×2 orthogonal matrices, and Σ represents a 2×2 diagonal matrix with non-negative real numbers. We then obtain the rotation matrix $R^* = UV^{\mathrm{T}}$. Using R^*, the position vector $\tilde{\boldsymbol{r}}_2^{(n)}$ is transformed to give $R^*\tilde{\boldsymbol{r}}_2^{(n)} + \bar{\boldsymbol{r}}_1$, which is a mapping from the coordinate system $x_2 - y_2$ to the coordinate system $x_1 - y_1$. Although we have discussed the special case where $M = 2$ above, a similar procedure can be performed in a general case, including cases where $M > 2$.

B. Proposed Data Fusion Method Using Respiratory Correlation and Procrustes Analysis

To apply Procrustes analysis to transform the coordinate systems of a multiradar system, the cluster positions can be used to form the input matrices S_1 and S_2. We should note here that Procrustes analysis requires at least two pairs of corresponding points, e.g., $(\boldsymbol{r}_1^{(1)}, \boldsymbol{r}_2^{(1)}), (\boldsymbol{r}_1^{(2)}, \boldsymbol{r}_2^{(2)})$. In this section, we propose a method to associate the cluster positions that uses the respiratory features of the human targets. In the proposed method, the similarity of the respiratory displacement waveforms is used to associate multiple echoes. The algorithmic steps for fusing data from multiple radar sensors are graphically presented in Fig. 2. The proposed method comprises the following five steps.

1) Two pairs of corresponding points are estimated using the correlation coefficient for the respiratory displacement waveforms. For the position vectors $\boldsymbol{r}_1^{(n_1)}$ and $\boldsymbol{r}_2^{(n_2)}$, the correlation coefficient is calculated as:

$$\rho_{\mathrm{c}}(n_1, n_2) = (1/\rho_0) \int \angle I_1(t, \boldsymbol{r}_1^{(n_1)}) \angle I_2(t, \boldsymbol{r}_2^{(n_2)}) \mathrm{d}t, \tag{4}$$

where ρ_0 is introduced for normalization. First, we find a pair (n_1^*, n_2^*) that maximizes $\rho_{\mathrm{c}}(n_1, n_2)$, where

$$(n_1^*, n_2^*) = \arg\max_{(n_1, n_2)} \rho_{\mathrm{c}}(n_1, n_2). \tag{5}$$

Then, we find another pair (n_1^{**}, n_2^{**}), where

$$(n_1^{**}, n_2^{**}) = \arg\max_{(n_1, n_2)} \rho_{\mathrm{c}}(n_1, n_2) \quad \text{subject to } n_1 \neq n_1^*, n_2 \neq n_2^*. \tag{6}$$

京都大学 KYOTO UNIVERSITY
A Self-archived copy in
Kyoto University Research Information Repository
https://repository.kulib.kyoto-u.ac.jp
京都大学学術情報リポジトリ KURENAI 紅 Kyoto University Research Information Repository

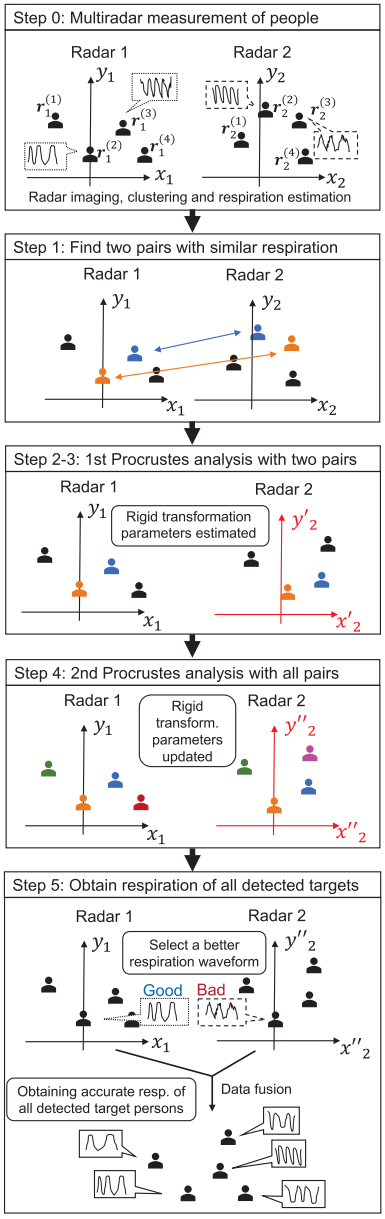

Fig. 2. Steps of the proposed method.

2) Procrustes analysis is applied to the two pairs of points (n_1^*, n_2^*) and (n_1^{**}, n_2^{**}), and the rigid transformation parameters R^* and $\boldsymbol{t}^*$ are then obtained.
3) Using R^* and $\boldsymbol{t}^*$, all position vectors $\boldsymbol{r}_m^{(n)}$ $(m = 1, \ldots, M; n = 1, \ldots, N)$ are transformed into the coordinate system x_1-y_1. All pairs of transformed points separated by a distance less than a threshold d_{th} are regarded as associated pairs, i.e.,

$$\left| \boldsymbol{r}_1^{(n_1)} - R^* \boldsymbol{r}_2^{(n_2)} - \boldsymbol{t}^* \right| \leq d_{\text{th}}. \tag{7}$$

4) All associated pairs are processed using Procrustes analysis, and the transformation parameters R^* and $\boldsymbol{t}^*$ are then updated.
5) For each human target, the displacement $\angle I_1(t, \boldsymbol{r}_1^{(n_1)}), \ldots, \angle I_M(t, \boldsymbol{r}_M^{(n_M)})$ that is most likely to reflect the target's respiratory motion is selected. We select the displacement that has a waveform that is closest to a sinusoidal wave. Using the following fourth-order moment of the power spectrum, we then find the m that maximizes $\kappa(n, m)$ for each n $(1 \leq n \leq N)$. We define

$$\kappa(n, m) = \frac{\int_0^\infty \left| \int_{-\infty}^\infty I_m(t, \boldsymbol{r}_m^{(n)}) \mathrm{e}^{-\mathrm{j}\omega t} \mathrm{d}t \right|^4 \mathrm{d}\omega}{\left| \int_0^\infty \left| \int_{-\infty}^\infty I_m(t, \boldsymbol{r}_m^{(n)}) \mathrm{e}^{-\mathrm{j}\omega t} \mathrm{d}t \right|^2 \mathrm{d}\omega \right|^2}, \tag{8}$$

and the optimum m is then found as

$$m^*(n) = \arg\max_m \kappa(n, m), \tag{9}$$

which means that the $m^*(n)$-th radar signal is used for the n-th human target. As a result, for each person, the displacement waveform that is most likely to be related to their respiration is selected, thus enabling their respiration to be accurately measured.

IV. Experimental Evaluation of the Proposed Method

A. Multiradar Experiment With Multiple People

We performed the experiments using both a pair of array radar systems and belt-type respirometers simultaneously to evaluate the accuracy of the multiradar-based respiratory measurements acquired using the proposed method. To evaluate the accuracy of the method in measuring the respiratory intervals, all participants wore a belt-type respirometer on their upper torso. Each participant was seated and breathing normally, and the measurements were acquired using two radar systems that were installed with different orientations and at different positions. Note that the belt-type respirometers were only used to evaluate the accuracy of the radar-based measurements.

Both radar systems are frequency-modulated continuous wave (FMCW) radar systems with a center frequency of 79 GHz, a center wavelength of $\lambda = 3.8$ mm, and an occupied bandwidth of 3.9 GHz. The beamwidths of the individual radar array elements are $\pm 4°$ and $\pm 35°$ in the E- and H-planes, respectively. The radar array is composed of a multiple-input multiple-output (MIMO) array that contains three transmitting and four receiving elements, with spacings of 7.6 mm (2λ) between the transmitting elements and spacings of 1.9 mm $(\lambda/2)$ between the receiving elements. In the experimental setting, the MIMO array can be approximated using a virtual linear array. Specifically, the array used in this study can be approximated using a 12-element virtual linear array with element spacings of $\lambda/2$. The slow-time sampling intervals were 100 ms.

Although the system includes two radar systems with the same configuration, we empirically confirmed that the interference between the systems was negligible. This negligible interference is partly because interference components are readily rejected by the clutter suppression process described in Section II. If signals arrive from other radar systems, these signals cannot be practically distinguished from static clutter components because they are mostly time independent if the distance between radar systems is fixed. In addition, the radar

京都大学 KYOTO UNIVERSITY
A Self-archived copy in
Kyoto University Research Information Repository
https://repository.kulib.kyoto-u.ac.jp
京都大学学術情報リポジトリ KURENAI 紅 Kyoto University Research Information Repository

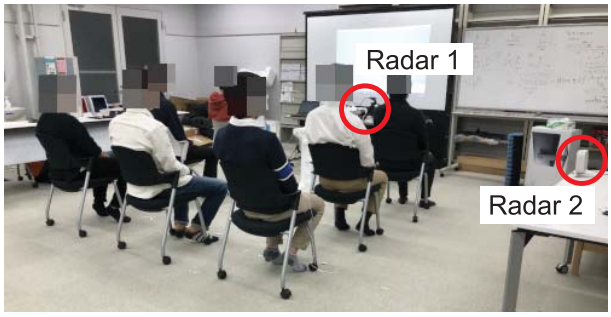

Fig. 3. Measurement setup with the seven seated participants shown with belt-type respirometer devices on their upper torsos in scenario 1.

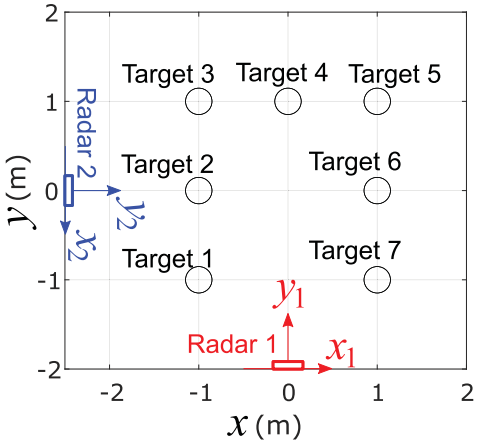

Fig. 4. Actual layout of the radar systems and participants in scenario 1.

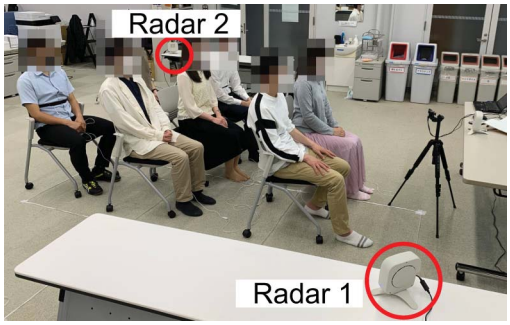

Fig. 5. Measurement setup with the seven seated participants shown with belt-type respirometer devices on their upper torsos in scenario 2.

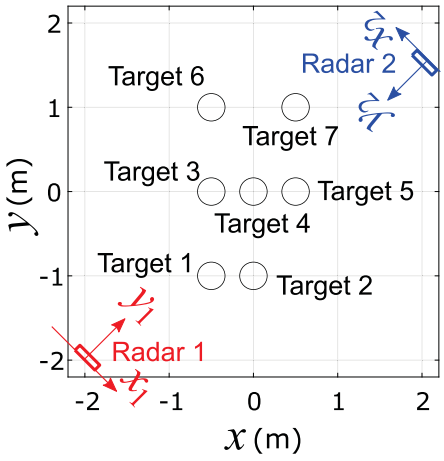

Fig. 6. Actual layout of the radar systems and participants in scenario 2.

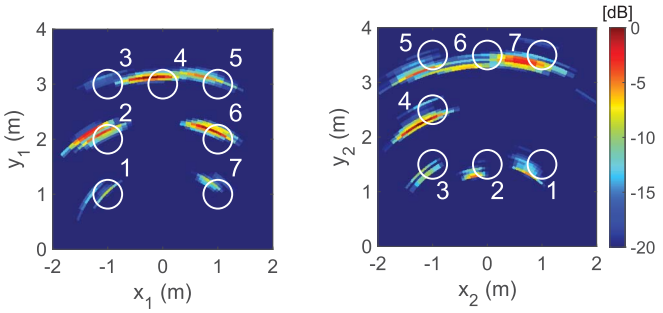

Fig. 7. Examples of radar images $|I_1(t, \boldsymbol{r}_1)|^2$ (left panel) and $|I_2(t, \boldsymbol{r}_2)|^2$ (right panel) at $t = 30$ s in scenario 1.

transmitters are active only for a short fraction of time in each cycle (approximately 13%), which means that signals from multiple radar systems do not always collide. For these reasons, we can expect our measured data to be practically free from interference.

We applied the proposed method to the radar data that were measured with the seven participants in two scenarios. We set different layouts for both the human targets and the radar systems in these scenarios. In scenario 1, as shown in Fig. 3, the seven participants were seated in a U-shaped arrangement with participant spacing of 1 m. We then used a pair of array radar systems to measure the participants as illustrated in Fig. 4. In scenario 2, the seven participants were seated in a different layout, as shown in Fig. 5, and the radar systems were placed at different positions with different orientations, as illustrated in Fig. 6. The measurement time was 120 s and the participants were instructed to remain still and breathe normally during the measurements. To evaluate the accuracy of the respiration measurements, belt-type contact respirometers were used simultaneously with the radar measurements.

B. Application of the Proposed Data Fusion Method to the Measured Radar Data

1) Application in Scenario 1: First, we applied the proposed method to the data acquired in scenario 1. The left and right panels of Fig. 7 show radar images $|I_1(t, \boldsymbol{r}_1)|^2$ and $|I_2(t, \boldsymbol{r}_2)|^2$ at $t = 30$ s. In the figure, the actual target positions are indicated by white circles with the target numbers. We note that in Fig. 7, the center of each circle is not aligned with the position with the locally highest intensity. This is because the radar echoes are reflected from a point on the surface of the human body that is not the same as the central position of the human body (as indicated by the white circle).

Next, a point cloud was generated from these images and the respiratory-space clustering algorithm [39] was then applied to generate the radar cluster images $C_1(t, \boldsymbol{r}_1)$ and $C_2(t, \boldsymbol{r}_2)$ shown in Fig. 8. In the figure, an alphabetical label is provided for each cluster. In image $|I_1(t, \boldsymbol{r}_1)|^2$ in Fig. 7, the echo from target 3 is barely visible because of shadowing; as a result, in Fig. 8, target 3 is not classified as a cluster. The resulting

京都大学 KYOTO UNIVERSITY
A Self-archived copy in
Kyoto University Research Information Repository
https://repository.kulib.kyoto-u.ac.jp
京都大学学術情報リポジトリ KURENAI 紅 Kyoto University Research Information Repository

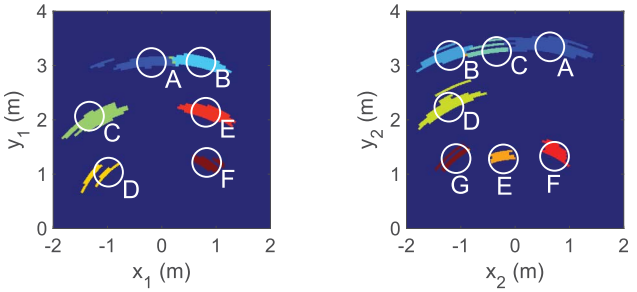

Fig. 8. Radar cluster images $C_1(t, \boldsymbol{r}_1)$ (left panel) and $C_2(t, \boldsymbol{r}_2)$ (right panel) at $t = 30$ s in scenario 1. The different colors represent different clusters.

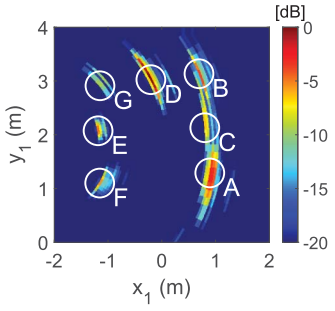

Fig. 9. Radar image $|\hat{I}_2(t, \boldsymbol{r}_1)|^2$ after the optimized rigid transformation has been performed in scenario 1.

TABLE II
CORRELATION COEFFICIENTS ρ FOR THE DISPLACEMENT WAVEFORMS IN SCENARIO 1

		Target index of radar 2						
		A	B	C	D	E	F	G
Target index of radar 1	A	0.13	0.63	0.02	0.15	0.01	0.17	0.07
	B	0.19	0.60	0.10	0.52	0.34	0.02	0.02
	C	0.20	0.05	0.04	0.03	0.81	0.01	0.01
	D	0.24	0.08	0.36	0.06	0.14	0.36	0.23
	E	0.18	0.07	0.89	0.04	0.15	0.13	0.80
	F	0.04	0.27	0.56	0.29	0.04	0.20	0.51

TABLE III
TARGET DETECTION RATES IN SCENARIO 1

	Participant number						
	1	2	3	4	5	6	7
Radar 1 (%)	100	100	0	100	100	100	100
Radar 2 (%)	100	100	100	100	100	69	100
Proposed (%)	100	100	100	100	100	100	100

TABLE IV
ERRORS IN RPM ESTIMATION WHEN USING THE PROPOSED METHOD

	Participant number						
	1	2	3	4	5	6	7
Scenario 1 (rpm)	0.43	0.02	0.06	0.88	0.72	0.05	0.15
Scenario 2 (rpm)	0.40	1.79	1.75	1.97	0.04	0.38	2.35

number of clusters was thus estimated erroneously to be six rather than seven, which is equivalent to the estimated number of human targets. This type of shadowing problem can occur particularly when multiple people are densely spaced within the measurement scene. To mitigate the shadowing problem, this study uses multiple radar systems rather than a single system.

Next, the proposed method was used to calculate the correlation coefficient ρ_C for each pair of displacement waveforms (see Table II). The proposed method finds two pairs of points with the largest and second largest values of ρ_C. In Table II, we can find the largest correlation coefficient for the pairing of target E (radar 1) and target C (radar 2). We can also find the second largest correlation coefficient for the pairing of target C (radar 1) and target E (radar 2). These pairs (E, C), (C, E) were processed via Procrustes analysis for $N = 2$, and the rigid transformation parameters $x = -2.52$ m, $y = 1.90$ m, and $\theta = -1.58$ rad were obtained.

Using these parameters, the radar image $|I_2(t, \boldsymbol{r}_2)|^2$ was then transformed into $|\hat{I}_2(t, \boldsymbol{r}_1)|^2$. Using the transformation parameters, the proposed method associated the six cluster pairs (A, D), (B, B), (C, E), (D, F), (E, C), and (F, A) from the seven human targets, where the distance threshold was set at $d_{\text{th}} = 0.5$ m. Note that cluster G from the second radar system was not associated in this process. The associated pairs were then processed via Procrustes analysis and the transformation parameters $x = -2.46$ m, $y = 1.86$ m, and $\theta = -1.57$ rad were updated, as illustrated in Fig. 9.

For the associated cluster pair (n_1, n_2), the respiratory displacement waveforms $\angle I_1(t, \boldsymbol{r}_1^{(n_1)})$ and $\angle I_2(t, \boldsymbol{r}_2^{(n_2)})$ were then obtained. We define the detection rate for each person as the percentage of time that the target person is detected out of all measurement time. The detection rate for 120 s for each target is shown in Table III. The table shows that human target 3 was not detected by one of the radar systems because of shadowing. All the human targets, with the exception of target 3, were detected by both radar systems, which gives us selection options; we can thus select a more accurate radar system for each target. In the proposed method, the fourth-order statistical parameter κ is calculated for both displacement waveforms over time duration T_κ, from which the waveform with the larger κ value is selected. Note that T_κ should be substantially longer than the typical respiratory interval (e.g., 3–5 s). At the same time, a short T_κ is preferable because it determines the update interval of the proposed method. Considering these factors, we selected $T_\kappa = 30$ s empirically.

Next, we evaluated the accuracy of the respiration rate estimation. The respiration rate is defined by the number of respirations per minute (rpm). The mean average error of the respiration rate for the k-th participant e_k $(k = 1, \ldots, 7)$ was calculated as $e_k = (1/L)\sum_{l=1}^{L} |r_{\text{e}}^{(k)}(t_l) - r_0^{(k)}(t_l)|$, where t_l $(l = 1, 2, \ldots, L)$ is the time sample, and L is the number of time samples corresponding to 120 s. In addition, $r_{\text{e}}^{(k)}(t)$ and $r_0^{(k)}(t)$ are the estimated and reference respiration rates, respectively, where the reference respiration rate was measured using the belt-type respirometer. Table IV shows the error e_k obtained when the two radar systems are combined. The error averaged over the seven participants is 0.33 rpm for the proposed process when combining the two radar systems. These results indicate that the proposed method using the multiradar system is effective in performing accurate respiration measurements of multiple people simultaneously.

京都大学 KYOTO UNIVERSITY
A Self-archived copy in
Kyoto University Research Information Repository
https://repository.kulib.kyoto-u.ac.jp
京都大学学術情報リポジトリ KURENAI 紅 Kyoto University Research Information Repository

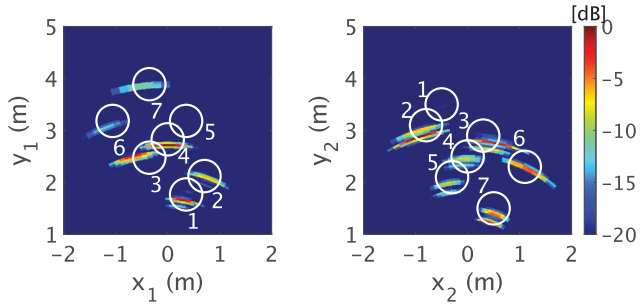

Fig. 10. Examples of radar images $|I_1(t, \boldsymbol{r}_1)|^2$ (left panel) and $|I_2(t, \boldsymbol{r}_2)|^2$ (right panel) at $t = 30$ s in scenario 2.

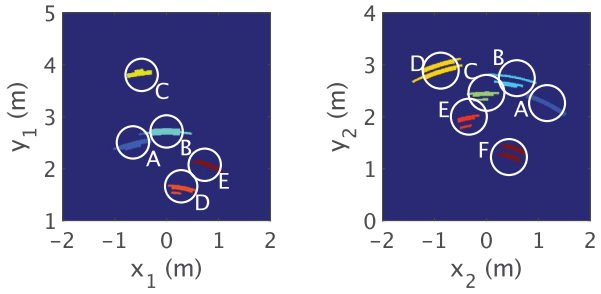

Fig. 11. Radar cluster images $C_1(t, \boldsymbol{r}_1)$ (left panel) and $C_2(t, \boldsymbol{r}_2)$ (right panel) at $t = 30$ s in scenario 2. The different colors represent different clusters.

TABLE V
CORRELATION COEFFICIENTS ρ FOR THE DISPLACEMENT WAVEFORMS IN SCENARIO 2

		Target index of radar 2					
		A	B	C	D	E	F
Target index of radar 1	A	0.27	0.38	0.14	0.22	0.03	0.38
	B	0.01	0.14	0.36	0.03	0.02	0.20
	C	0.25	0.42	0.18	0.38	0.11	0.44
	D	0.31	0.04	0.29	0.21	0.35	0.15
	E	0.09	0.07	0.08	0.29	0.07	0.17

2) Application in Scenario 2: We also applied the proposed method to the radar data acquired in scenario 2. The layout of the target people in this case is shown in Fig. 6. Using radar systems 1 and 2, the radar images $|I_1(t, \boldsymbol{r}_1)|^2$ and $|I_2(t, \boldsymbol{r}_2)|^2$ were generated as shown in Fig. 10. We can then generate the radar cluster images $C_1(t, \boldsymbol{r}_1)$ and $C_2(t, \boldsymbol{r}_2)$ shown in Fig. 11. In Fig. 11, no clusters were generated for targets 5 and 6 because the echoes from targets 5 and 6 are weak in image $|I_1(t, \boldsymbol{r}_1)|^2$, as shown in Fig. 10. Similarly, no cluster was generated for target 1 because the echo is weak in image $|I_2(t, \boldsymbol{r}_2)|^2$, as shown in Fig. 10.

The proposed method was then used to calculate the correlation coefficient ρ_C for each of the pairs of displacement waveforms (Table V). In Table V, we find that the largest correlation coefficient is that for the pairing of target C (radar 1) and target F (radar 2), and also find that the second largest correlation coefficient is that for the pairing of target A (radar 1) and target B (radar 2). These pairs, denoted by (C, F), (A, B), were processed via Procrustes analysis for $N = 2$, and the rigid transformation parameters $x = -0.17$ m, $y = 5.11$ m, and $\theta = -3.07$ rad were obtained.

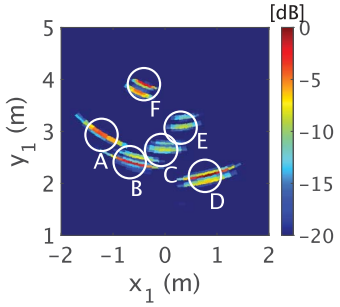

Fig. 12. Radar image $|\hat{I}_2(t, \boldsymbol{r}_1)|^2$ after the optimized rigid transformation has been performed in scenario 2.

TABLE VI
TARGET DETECTION RATES IN SCENARIO 2

	Participant number						
	1	2	3	4	5	6	7
Radar 1 (%)	100	100	100	100	0	58	72
Radar 2 (%)	0	100	100	100	100	100	100
Proposed (%)	100	100	100	100	100	100	100

Then, using these parameters, the radar image $|I_2(t, \boldsymbol{r}_2)|^2$ was transformed into $|\hat{I}_2(t, \boldsymbol{r}_1)|^2$. Using the transformation parameters, the proposed method associated the four cluster pairs (A, B), (B, C), (C, F), and (E, D) from the clusters. Note that cluster D from the first radar system and clusters A and E from the second radar system were not associated in this process. Using the associated pairs, the transformation parameters $x = 0.12$ m, $y = 5.09$ m, and $\theta = 3.06$ rad were updated, as illustrated in Fig. 12.

For the associated cluster pair (n_1, n_2), the respiratory displacement waveforms $\angle I_1(t, \boldsymbol{r}_1^{(n_1)})$ and $\angle I_2(t, \boldsymbol{r}_2^{(n_2)})$ were obtained. The respiration detection rates for each target when using the proposed method are shown in Table VI, which shows that human targets 1 and 5 were only detected by one of the two radar systems because of shadowing, whereas the other targets were detected by both radar systems. Table IV shows the errors in respiration rate estimation when using the proposed data fusion technique for these radar systems. The average error for the seven participants was 1.24 rpm when using the proposed method to combine the radar data.

The errors in estimating the respiration rate in scenarios 1 and 2 were 0.33 and 1.24 rpm, respectively. The reason for the different accuracies in these scenarios is partly explained by the layout of participants; in scenario 1, the distances between adjacent participants were all 1.0 m, whereas in scenario 2, the minimum distance between participants was 0.5 m. The densely located participants in scenario 2 made the respiratory measurement more challenging, resulting in a larger error. Despite this, the error values in both scenarios were much smaller than the typical respiration rate 12–20 rpm of healthy adults, which demonstrates the effectiveness of the proposed method.

V. DISCUSSION

A. Performance of the Proposed Method With Various Parameter Settings

First, we evaluated the accuracy of the proposed method in estimating the rigid transformation parameters for different threshold values d_{th} in Eq. (7). Table VII shows the accuracy

京都大学 KYOTO UNIVERSITY
A Self-archived copy in
Kyoto University Research Information Repository
https://repository.kulib.kyoto-u.ac.jp
京都大学学術情報リポジトリ KURENAI 紅 Kyoto University Research Information Repository

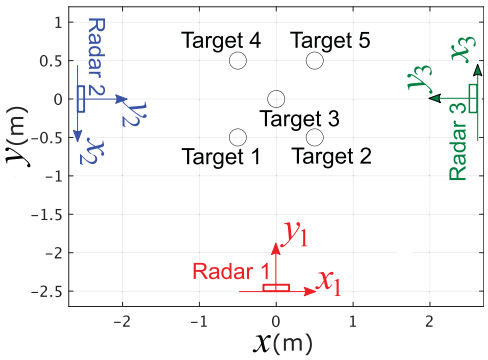

Fig. 13. Actual layout of the radar systems and participants in scenario 3.

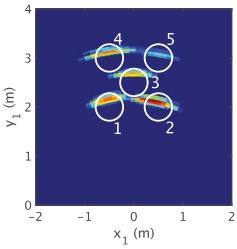

(a) Radar 1

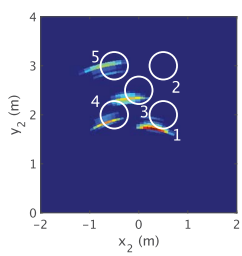

(b) Radar 2

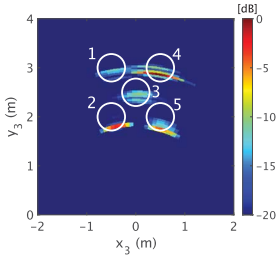

(c) Radar 3

Fig. 14. Examples of radar images $|I_1(t, \boldsymbol{r}_1)|^2$ (a), $|I_2(t, \boldsymbol{r}_2)|^2$ (b), and $|I_3(t, \boldsymbol{r}_3)|^2$ (c), for $t = 30$ s in scenario 3.

of the proposed method for $d_{\text{th}} = 0.2$, 0.5, and 1.0 m, in scenario 1. In the table, the errors are $\Delta x = |x_{\text{e}} - x_0|$, $\Delta y = |x_{\text{e}} - y_0|$, and $\Delta\theta = |\theta_{\text{e}} - \theta_0|$, where x_{e}, y_{e}, and θ_{e} are the estimated parameters, and $x_0 = -2.5$ m, $y_0 = 2.0$ m, and $\theta_0 = -90°$ are the actual values. Note that the second row of the table corresponds to the result discussed in the previous section. For a small d_{th}, the parameters are determined mostly by the first Procrustes analysis, which lowers the accuracy, whereas for a large d_{th}, incorrect pairs of points may be used in the second Procrustes analysis, which also lowers the accuracy. In the proposed method, d_{th} was set to 0.5 m to take into account these factors.

Next, we evaluate the accuracy of the proposed method in scenario 1 for different radar frequency bandwidths (BWs). Although the original radar BW is 3.9 GHz, the effective BW can be reduced by numerically restricting the data length in the frequency domain. Table VIII shows the estimation errors Δx, Δy, and $\Delta\theta$ for the BWs of 0.1, 0.2, 0.3, 1.5, and 3.9 GHz, which correspond to the range resolution $\Delta r = 1.50$, 0.75, 0.50, 0.10, and 0.04 m, respectively. As shown in the table, the proposed method can estimate the parameters with sufficient accuracy even when the range resolution is set to 0.50 m, whereas the estimation error increases to

TABLE VII
PARAMETER ESTIMATION ERROR FOR VARIOUS d_{th} VALUES

d_{th}(m)	Δx (m)	Δy (m)	$\Delta\theta$ (deg)
0.2	0.0	0.0	2.6
0.5	0.0	0.1	0.0
1.0	0.0	0.5	5.3

TABLE VIII
PARAMETER ESTIMATION ERROR FOR VARIOUS BWs

BW (GHz)	Δr (m)	Δx (m)	Δy (m)	$\Delta\theta$ (deg)
0.1	1.50	2.4	1.5	90.0
0.2	0.75	2.4	1.2	90.0
0.3	0.50	0.0	0.1	0.9
1.5	0.10	0.0	0.1	0.5
3.9	0.04	0.0	0.1	0.0

TABLE IX
TARGET DETECTION RATES IN SCENARIO 3

	Participant number				
	1	2	3	4	5
Radar 1 alone (%)	100	100	92	94	58
Radar 2 alone (%)	100	0	100	100	100
Radar 3 alone (%)	0	100	100	100	100
Proposed with radar 1 & 2 (%)	100	100	100	100	100
Proposed with radar 2 & 3 (%)	100	100	100	100	100
Proposed with radar 3 & 1 (%)	100	100	100	100	100

an unacceptable level when the range resolution is set to 0.75 and 1.50 m.

B. Performance of the Proposed Method With Densely Located People

We performed an additional measurement with five participants using three radar systems with different orientations (scenario 3), as shown in Fig. 13. The distance between adjacent participants was set to 0.7 m. Using radar systems 1, 2, and 3, the radar images $|I_1(t, \boldsymbol{r}_1)|^2$, $|I_2(t, \boldsymbol{r}_2)|^2$, and $|I_3(t, \boldsymbol{r}_3)|^2$ were generated as in Fig. 14, which shows that some of the target persons are invisible in the images. For example, the echo from target 5 is weak in $|I_1(t, \boldsymbol{r}_1)|^2$ in Fig. 14 (a), and no echo is seen from target 2 in $|I_2(t, \boldsymbol{r}_2)|^2$ in Fig. 14 (b). We used two of the three radar systems to evaluate the performance of the proposed method. The detection rate for each target is shown in Table IX. As shown in the table, although some of the participants were not always detected by a single radar, the proposed method can resolve the shadowing issue using any two of the three radar systems, and all participants were detected for the whole measurement time of 100 s. Further measurements with different numbers of participants as well as different layouts of radar systems and participants are needed to confirm the applicability of the proposed method in realistic scenarios, which is out of the scope of this paper and left as work for future projects.

VI. CONCLUSION

In this study, we have proposed a novel method for a multiradar system that can measure the positions and respiration characteristics of multiple people. By introducing multiple

京都大学 KYOTO UNIVERSITY
A Self-archived copy in
Kyoto University Research Information Repository
https://repository.kulib.kyoto-u.ac.jp
京都大学学術情報リポジトリ KURENAI 紅 Kyoto University Research Information Repository

radar systems rather than a single system, the shadowing problem can be mitigated, which means that the respiration rates of multiple people can be measured even when these people are located closely together. In addition, when using multiple radar systems, we can measure each person from multiple directions, which improves the accuracy of the respiration measurements. The effectiveness of the proposed method was verified experimentally in two scenarios using a pair of radar systems and seven participants.

In both scenarios, the proposed method was demonstrated to be able to detect all participants by combining the data acquired from the two radar systems, whereas not all participants could be detected when using only one of the two radar systems because of shadowing. The average respiratory rate estimation error for the seven participants in the two scenarios was 0.79 rpm, which is sufficiently small when compared with the typical respiration rate range for adults (12-20 rpm). Use of the multiradar system with the proposed method has been demonstrated to be promising for use in accurate noncontact monitoring of the respiration of multiple people.

To address the main challenges that remain, our next steps are to extend the proposed method to 1) suppress the effect of unwanted body movements that can happen in realistic scenarios (e.g., in offices, schools, and hospitals) and 2) enable it to combine data from more than two radar systems to increase the number of target people that can be monitored.

Acknowledgment

The authors thank Dr. Hirofumi Taki and Dr. Shigeaki Okumura of MaRI Company, Ltd., for their help with this study. A preprint of this manuscript has been posted on arXiv (arXiv:2107.11525 [eess.SP]).

References

[1] M. Ali, A. Elsayed, A. Mendez, Y. Savaria, M. Sawan, and M. Sawan, "Contact and remote breathing rate monitoring techniques: A review," *IEEE Sensors J.*, vol. 21, no. 13, pp. 14569–14586, Jul. 2021.

[2] C. Massaroni, A. Nicolo, M. Sacchetti, and E. Schena, "Contactless methods for measuring respiratory rate: A review," *IEEE Sensors J.*, vol. 21, no. 11, pp. 12821–12839, Jun. 2021.

[3] A. Singh, S. U. Rehman, S. Yongchareon, and P. H. J. Chong, "Multi-resident non-contact vital sign monitoring using radar: A review," *IEEE Sensors J.*, vol. 21, no. 4, pp. 4061–4084, Feb. 2021.

[4] L. Storrer *et al.*, "Experimental implementation of a multi-antenna 802.11 ax-based passive bistatic radar for human target detection," in *Proc. IEEE Radar Conf.*, Florence, Italy, Sep. 2020, pp. 1–6.

[5] A. Abuduaini, N. Shiraki, N. Honma, T. Nakayama, and S. Iizuka, "Performance evaluation of multiple human-body localization using bistatic MIMO radar," in *Proc. IEEE Asia–Pacific Microw. Conf. (APMC)*, Singapore, Dec. 2019, pp. 575–577.

[6] T. Ha and J. Kim, "Detection and localization of multiple human targets based on respiration measured by IR-UWB radars," in *Proc. IEEE SENSORS*, Montreal, QC, Canada, Oct. 2019, pp. 1–4.

[7] N. Honma, D. Sasakawa, N. Shiraki, T. Nakayama, and S. Iizuka, "Human monitoring using MIMO radar," in *Proc. IEEE Int. Workshop Electromagn., Appl. Student Innov. Competition (iWEM)*, Nagoya, Japan, Aug. 2018, pp. 1–2.

[8] G. Shingu, K. Takizawa, and T. Ikegami, "Human body detection using MIMO-UWB radar sensor network in an indoor environment," in *Proc. 9th Int. PDCAT*, Dunedin, New Zealand, Dec. 2008, pp. 437–442.

[9] J. W. Choi, D. H. Yim, and S. H. Cho, "People counting based on an IR-UWB radar sensor," *IEEE Sensors J.*, vol. 17, no. 17, pp. 5717–5727, Sep. 2017.

[10] S. S. Ram, Y. Li, A. Lin, and H. Ling, "Human tracking using Doppler processing and spatial beamforming," in *Proc. IEEE Radar Conf.*, Waltham, MA, USA, Apr. 2007, pp. 546–551.

[11] D. Sasakawa, N. Honma, K. Nishimori, T. Nakayama, and I. Shoichi, "Evaluation of fast human localization and tracking using MIMO radar in multi-path environment," in *Proc. IEEE 27th Annu. Int. Symp. Pers., Indoor, Mobile Radio Commun. (PIMRC)*, Valencia, Spain, Sep. 2016, pp. 1–6.

[12] S. Chang, R. Sharan, M. Wolf, N. Mitsumoto, and J. W. Burdick, "UWB radar-based human target tracking," in *Proc. IEEE Radar Conf.*, Pasadena, CA, USA, May 2009, pp. 1–6.

[13] Y. He, F. Le Chevalier, and A. G. Yarovoy, "Association of range-Doppler video sequences in multistatic UWB radar for human tracking," in *Proc. 9th Eur. Radar Conf.*, Amsterdam, The Netherlands, Nov. 2012, pp. 218–221.

[14] A. E. Mitchell, G. E. Smith, K. L. Bell, and M. Rangaswamy, "Single target tracking with distributed cognitive radar," in *Proc. IEEE Radar Conf.*, Seattle, WA, USA, May 2017, pp. 285–288.

[15] J. Rovnakova and D. Kocur, "Data fusion from UWB radar network: Preliminary experimental results," in *Proc. 21st Int. Conf. Radioelektronika*, Brno, Czech Republic, Apr. 2011, pp. 1–4.

[16] G. L. Charvat, J. Goodwin, M. Tobias, J. Pozderac, and J. Peabody, "Detection algorithm implementation and measured results for a real-time, through-wall radar system using a TDM MIMO antenna array," in *Proc. IEEE Radar Conf.*, Atlanta, GA, USA, May 2012, pp. 240–246.

[17] M. Shin and H. Son, "Multiple sensor linear multi-target integrated probabilistic data association for ultra-wide band radar," *IEEE Access*, vol. 8, pp. 227161–227171, 2020.

[18] J. E. Kiriazi, S. M. M. Islam, O. Borić-Lubecke, and V. M. Lubecke, "Sleep posture recognition with a dual-frequency cardiopulmonary Doppler radar," *IEEE Access*, vol. 9, pp. 36181–36194, 2021.

[19] L. Li, R. Zhu, H. Li, and J. Zhou, "Human posture recognition based on multi-channel SAR at 77 GHz," in *Proc. IEEE 2nd Int. Conf. Automat., Electron. Electr. Eng. (AUTEEE)*, Shenyang, China, Nov. 2019, pp. 559–563.

[20] H. Cui and N. Dahnoun, "Human posture capturing with millimetre wave radars," in *Proc. 9th Medit. Conf. Embedded Comput. (MECO)*, Budva, Montenegro, Jun. 2020, pp. 1–4.

[21] Y. Wang, Q. Liu, and A. E. Fathy, "Simultaneous localization and respiration detection of multiple people using low cost UWB biometric pulse Doppler radar sensor," in *IEEE MTT-S Int. Microw. Symp. Dig.*, Montreal, QC, Canada, Jun. 2012, pp. 1–3.

[22] Q. Wu, Z. Mei, Z. Lai, D. Li, and D. Zhao, "A non-contact vital signs detection in a multi-channel 77 GHz LFMCW radar system," *IEEE Access*, vol. 9, pp. 49614–49628, 2021.

[23] D.-M. Chian, C.-K. Wen, F.-K. Wang, and K.-K. Wong, "Signal separation and tracking algorithm for multi-person vital signs by using Doppler radar," *IEEE Trans. Biomed. Circuits Syst.*, vol. 14, no. 6, pp. 1346–1361, Dec. 2020.

[24] O. Boric-Lubecke, V. M. Lubecke, A. Host-Madsen, D. Samardzija, and K. Cheung, "Doppler radar sensing of multiple subjects in single and multiple antenna systems," in *Proc. 7th Int. Conf. Telecommun. Mod. Satell., Cable Broadcast. Services*, Nis, Serbia, vol. 1, Sep. 2005, pp. 7–11.

[25] Y. Chen, H. Tan, B. Hu, and Y. Li, "Doppler radar based non-contact multi-person respiration signals separation," in *Proc. IEEE-EMBS Int. Conf. Biomed. Health Inform.*, Hong Kong, Jan. 2012, pp. 799–802.

[26] S. M. M. Islam, E. Yavari, A. Rahman, V. M. Lubecke, and O. Boric-Lubecke, "Separation of respiratory signatures for multiple subjects using independent component analysis with the JADE algorithm," in *Proc. 40th Annu. Int. Conf. IEEE Eng. Med. Biol. Soc. (EMBC)*, Honolulu, HI, USA, Jul. 2018, pp. 1234–1237.

[27] N. V. Rivera, S. Venkatesh, C. Anderson, and R. M. Buehrer, "Multi-target estimation of heart and respiration rates using ultra wideband sensors," in *Proc. 14th Eur. Signal Process. Conf.*, Florence, Italy, Sep. 2006, pp. 1–6.

[28] M. Muragaki *et al.*, "Noncontact respiration monitoring of multiple closely positioned patients using ultra-wideband array radar with adaptive beamforming technique," in *Proc. IEEE ICASSP*, New Orleans, LA, USA, Mar. 2017, pp. 1118–1122.

[29] C. Lu, Y. Yuan, C.-H. Tseng, and C.-T. M. Wu, "Multi-target continuous-wave vital sign radar using 24 GHz metamaterial leaky wave antennas," in *IEEE MTT-S Int. Microw. Symp. Dig.*, Nanjing, China, May 2019, pp. 1–4.

[30] C. Ding, J. Yan, L. Zhang, H. Zhao, H. Hong, and X. Zhu, "Noncontact multiple targets vital sign detection based on VMD algorithm," in *Proc. IEEE Radar Conf.*, Seattle, WA, USA, May 2017, pp. 0727–0730.

[31] H. Lv *et al.*, "Multi-target human sensing via UWB bio-radar based on multiple antennas," in *Proc. IEEE Region Conf. (TENCON)*, Xi'an, China, Oct. 2013, pp. 1–4.

京都大学 KYOTO UNIVERSITY
A Self-archived copy in
Kyoto University Research Information Repository
https://repository.kulib.kyoto-u.ac.jp
京都大学学術情報リポジトリ KURENAI 紅 Kyoto University Research Information Repository

[32] A. Rittiplang and P. Phasukkit, "UWB radar for multiple human detection through the wall based on Doppler frequency and variance statistic," in *Proc. 12th Biomed. Eng. Int. Conf. (BMEiCON)*, Ubon Ratchathani, Thailand, Nov. 2019, pp. 1–5.
[33] J. Yan, H. Hong, H. Zhao, Y. Li, C. Gu, and X. Zhu, "Through-wall multiple targets vital signs tracking based on VMD algorithm," *Sensors*, vol. 16, no. 8, p. 1293, Aug. 2016.
[34] I. Walterscheid, O. Biallawons, and P. Berens, "Contactless respiration and heartbeat monitoring of multiple people using a 2-D imaging radar," in *Proc. 41st Annu. Int. Conf. IEEE Eng. Med. Biol. Soc. (EMBC)*, Berlin, Germany, Jul. 2019, pp. 3720–3725.
[35] J. Xiong, H. Hong, H. Zhang, N. Wang, H. Chu, and X. Zhu, "Multi-target respiration detection with adaptive digital beamforming technique based on SIMO radar," *IEEE Trans. Microw. Theory Techn.*, vol. 68, no. 11, pp. 4814–4824, Nov. 2020.
[36] M. Nosrati, S. Shahsavari, S. Lee, H. Wang, and N. Tavassolian, "A concurrent dual-beam phased-array Doppler radar using MIMO beamforming techniques for short-range vital-signs monitoring," *IEEE Trans. Antennas Propag.*, vol. 67, no. 4, pp. 2390–2404, Apr. 2019.
[37] S. M. M. Islam, O. Boric-Lubecke, and V. M. Lubekce, "Concurrent respiration monitoring of multiple subjects by phase-comparison monopulse radar using independent component analysis (ICA) with JADE algorithm and direction of arrival (DOA)," *IEEE Access*, vol. 8, pp. 73558–73569, 2020.
[38] W. C. Su, M. C. Tang, R. El Arif, T. S. Horng, and F.-K. Wang, "Stepped-frequency continuous-wave radar with self-injection-locking technology for monitoring multiple human vital signs," *IEEE Trans. Microw. Theory Techn.*, vol. 67, no. 12, pp. 5396–5405, Dec. 2019.
[39] T. Koda, T. Sakamoto, S. Okumura, and H. Taki, "Noncontact respiratory measurement for multiple people at arbitrary locations using array radar and respiratory-space clustering," *IEEE Access*, early access, Jul. 26, 2021, doi: 10.1109/ACCESS.2021.3099821.
[40] X. Shang, J. Liu, and J. Li, "Multiple object localization and vital sign monitoring using IR-UWB MIMO radar," *IEEE Trans. Aerosp. Electron. Syst.*, vol. 56, no. 6, pp. 4437–4450, Dec. 2020.
[41] Y. Yang, J. Cao, X. Liu, and X. Liu, "Multi-breath: Separate respiration monitoring for multiple persons with UWB radar," in *Proc. IEEE 43rd Annu. Comput. Softw. Appl. Conf. (COMPSAC)*, Milwaukee, WI, USA, Jul. 2019, pp. 840–849.
[42] S. Iwata, T. Koda, and T. Sakamoto, "Multiradar data fusion for respiratory measurement of multiple people," 2021, *arXiv:2107.11525*. [Online]. Available: http://arxiv.org/abs/2107.11525
[43] D. Pelleg and A. Moore, "*X*-means: Extending *K*-means with efficient estimation of the number of clusters," in *Proc. 17th Int. Conf. Mach. Learn.*, Stanford, CA, USA, Jun. 2000, pp. 727–734.
[44] J. M. F. T. Berge, J. C. Gower, and G. B. Dijksterhuis, "Procrustes problems," in *Psychometrika*, vol. 70. New York, NY, USA: Oxford Univ. Press, Dec. 2005, pp. 799–801.
[45] S. Rusinkiewicz and M. Levoy, "Efficient variants of the ICP algorithm," in *Proc. 3rd Int. Conf. 3-D Digit. Imag. Model.*, Quebec City, QC, Canada, May 2001, pp. 145–152.

Shunsuke Iwata (Member, IEEE) received the B.E. degree in electrical and electronic engineering from Kyoto University, Kyoto, Japan, in 2021, where he is currently pursuing the M.E. degree in electrical engineering with the Graduate School of Engineering. His research interest includes multiradar measurement of respiration of multiple people. Mr. Iwata was a recipient of the 2020 IEEE AP-S Kansai Joint Chapter Best Presentation Award.

Takato Koda received the B.E. degree in electrical and electronic engineering from Kyoto University, Kyoto, Japan, in 2020, where he is currently pursuing the M.E. degree in electrical engineering with the Graduate School of Engineering. His research interests include radar imaging and clustering of multiple people using array radar systems.

Takuya Sakamoto (Senior Member, IEEE) received the B.E. degree in electrical and electronic engineering from Kyoto University, Kyoto, Japan, in 2000, and the M.I. and Ph.D. degrees in communications and computer engineering from the Graduate School of Informatics, Kyoto University, in 2002 and 2005, respectively.

From 2006 to 2015, he was an Assistant Professor at the Graduate School of Informatics, Kyoto University. From 2011 to 2013, he was a Visiting Researcher at Delft University of Technology, Delft, The Netherlands. From 2015 to 2018, he was an Associate Professor at the Graduate School of Engineering, University of Hyogo, Himeji, Japan. In 2017, he was a Visiting Scholar at the University of Hawaii at Manoa, Honolulu, HI, USA. Since 2018, he has been a PRESTO Researcher at Japan Science and Technology Agency, Kawaguchi, Japan. At present, he is an Associate Professor at the Graduate School of Engineering, Kyoto University. His current research interests are system theory, inverse problems, radar signal processing, radar imaging, and wireless sensing of vital signs.

Dr. Sakamoto was a recipient of the Best Paper Award from the International Symposium on Antennas and Propagation (ISAP) in 2012 and Masao Horiba Award in 2016. In 2017, he was invited as a Semi-Plenary Speaker to the European Conference on Antennas and Propagation (EuCAP), Paris, France.